Proceedings of ASME Turbo Expo 2011
GT2011
June 6-10, 2011, Vancouver, British Columbia, Canada

GT2011-45242

EDDY CURRENT DAMPER FOR TURBINE BLADING: ELECTROMAGNETIC FINITE ELEMENT ANALYSIS AND MEASUREMENT RESULTS

Jacob Laborenz*
Malte Krack
Lars Panning
Jörg Wallaschek
Institute of Dynamics and Vibration Research
Leibniz Universität Hannover
30167 Hannover, Germany
Email: laborenz@ids.uni-hannover.de

Markus Denk
Pierre-Alain Masserey
ALSTOM Power
Steam Turbines and Generators
5401 Baden, Switzerland
Email: markus.denk@power.alstom.com

ABSTRACT

In the dynamics of turbomachinery the mechanical damping of the blading is in the focus of research for the last decades to improve the dynamic performance in terms of high cycle fatigue issues. Besides that an increased mechanical damping can produce a higher flutter safety margin such that stable operation conditions are achievable in a bigger range. Hence, novel damping techniques are considered besides the well known friction based damping devices.
In this paper an extended analysis of the eddy current based damping device for a last stage steam turbine blading presented in GT2009-59593 is conducted. A transient electromagnetic finite element analysis of the eddy current damper is performed and the resulting damping forces are compared to their analytical solution. Parameter studies are carried out and equivalent damping factors are calculated. Furthermore, for the validation of the finite element model a test rig was built which allows for the direct measurement of damping forces when forcing a sinusoidal relative motion. Forced response measurements and simulations are used to demonstrate its dynamic performance and predictability.

*Address all correspondence to this author.

NOMENCLATURE

a	air gap
B	Flux density
c_{eqv}	Equivalent stiffness
d_{eqv}	Equivalent damping constant
E	Electric field
$\mathbf{e}$	Unit vector
F	Force
F_{mag}	Static repellent force of permanent magnets
J	Current density
L	Magnet length
M_0	Permanent magnet magnetization
r_{c}	Copper plate radius
r_{mag}	Magnet radius
V	Volume
v	Velocity
β	Amplitude ratio: Vibration amplitude in relation to static air gap
δ	Copper plate thickness
σ	Conductivity
τ	Normalized time

1 INTRODUCTION

In the dynamics of turbomachinery the mechanical damping of the blading is in the focus of research for the last decades.

Due to high centrifugal loads and dynamic excitation forces the prevention of high cycle fatigue issues caused by static stress in connection with high vibrations amplitudes is of great importance. In case of designs with less contact interfaces, e.g. bladed disc assemblies and structures with very low internal damping, additional damping has to be applied in order to avoid high response levels at forced excitation near resonance.

For thirty years friction damping technologies are applied to turbine blades to improve their dynamic behavior [1]. In this approach vibration amplitude reduction is obtained through energy dissipation in friction contacts. Besides blade-to-blade [2] or blade-to-root [3] contact a broad variety of coupling devices such as underplatform dampers [4], [5], lacing wires and friction rings [6] have been studied in great detail during the last couple of years. To include those friction forces in vibration analyses, sophisticated contact models are necessary [7], [8], most of them containing parameters which are difficult to estimate such as contact stiffness [9] and friction coefficient. In the majority of the publications dealing with friction damping it becomes apparent that the contact parameters such as normal loading and friction coefficient have to be tuned carefully to achieve the best damper performance. Unfortunately they might change in operation condition, e.g. the friction coefficient depends on the temperature [10] and may alter through wear [11] resulting in unexpected vibration levels.

Therefore, besides the commonly used friction based damping devices, different damping techniques are within the scope of research. For instance DUFFY ET AL. [12] proposed an impact damper for turbine blades which consists of a steel ball in a cavity built in the blade. Amplitude reduction is achieved through impact losses between the ball and the cavities' walls in case of vibrations. They state an amplitude reduction of about 50% for a low-pressure turbine blade.

SUN ET AL. [13] examined the increase of material damping due to aluminum and epoxy coatings on steel and titanium compressor blades. They stated that the material damping could be increased by a factor of ten in the best case but that deeper analyses have to be carried out to give more accurate prediction. FILIPPI ET AL. [14] derived a methodology to account for the nonlinear behavior of coated turbine blades. An amplitude dependency of Young's modulus and loss factor was observed. A considerable decrease of the blade's Q-factor was achieved in the experiments and finite element results were in good agreement with the measurements. YEN ET AL. [15] studied the influence of a magnetomechanical coating on the vibration behavior of beams and blades. In this approach energy dissipation is achieved through irreversible movement of magnetic domain boundaries when straining the coating. A significant stress and amplitude reduction for higher vibration modes could be shown. DUFFY ET AL. [16] examined the influence of shunted piezoelectric patches applied to centrifugally loaded plates. In this approach vibrations are transformed into electrical energy in the piezoelectric patches which again is dissipated into heat in the shunt resistance. They state that piezoelectric material had the ability to reduce plate vibrations in the rotating frame. However, more sophisticated circuits should be used to improve performance. HOHL ET AL. [17] studied the effectiveness of piezoceramics with different shunt strategies when applied to a model blisk. In experiments a considerable amplitude reduction could be demonstrated when forcing with an engine order excitation. Simulated and measured forced response were in very good agreement when including the piezoelectric material and shunting in a mixed electrical/mechanical modal condensed model of the blade.

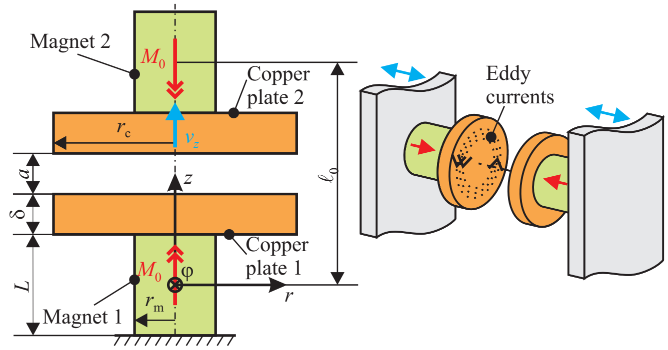

FIGURE 1. SCHEMATIC SKETCH OF DAMPING ELEMENT CONSISTING OF PERMANENT MAGNETS AND COPPER PLATES

In [18] an eddy current based damping device for last stage steam turbine blades was presented. In this non-contacting approach permanent magnets and copper plates are embedded into the blades facing each other between adjacent blades (see Fig. 1). In case of vibrations the relative movement between magnets and copper plates induces eddy currents in the conducting material such that mechanical energy is converted to electrical which then dissipates into heat and, therefore, leads to an amplitude reduction. To account for the damping element in structural analyses equivalent damping coefficients and stiffness were obtained by applying electromagnetic-mechanical laws. Forced response measurements and simulations of a dummy blade pair equipped with the damping element have been carried out and a considerable amplitude reduction was observed. Simulations utilizing the equivalent parameters match qualitatively the forced response measurements.

As the electromagnetic model established in [18] is restricted to some assumptions regarding geometry and boundary conditions, in this paper an extended analysis of the eddy current damper is conducted. A transient electromagnetic finite element analysis of the eddy current damping device is performed and the resulting damping forces are compared to their analytical solution. Parameter studies are carried out and equivalent damping factors are calculated. Furthermore, for the validation of the finite element model a test rig was built which allows for the direct measurement of damping forces when forcing a sinusoidal relative motion. Forced response measurements and simulations of the test rig presented in [18] are used to demonstrate its dynamic performance and predictability.

2 MATHEMATICAL MODEL OF THE EDDY CURRENT DAMPING DEVICE

In [18] an analytical model of the damping device was already presented. However, for the sake of completeness and to allow referencing to those equations they shall be summarized briefly. To obtain a simple model an axially rotational problem is regarded. That is, magnets and copper plates are of rotational symmetrical shape and movement is only considered in axial direction resulting in a magnetic flux with components unequal to zero only in radial and axial direction and eddy currents only circling in tangential direction. In order to obtain a closed form solution, it is necessary to assume a constant permeability μ within the problem region. Hence, vacuum is considered for the whole region. Also the influence of the induced eddy currents' magnetic field on the causative permanent magnets' field is neglected resulting in a linear set of equations.
Due to linearity the magnet array's flux density can be superimposed using the field of two single permanent magnets

$$\mathbf{B} = \mathbf{B}_1 + \mathbf{B}_2 \,. \tag{1}$$

An analytical expression based on Elliptical integrals for the single magnet's flux density is given in the Appendix (Eq. 13). In the derivation of the damping forces the upper half of the damping element depicted in Fig. 1 is regarded as moving with a velocity v_z in axial direction whereas the lower half is regarded as stationary. Hence, due to movement relative to the stationary part of the magnetic field $\mathbf{B}_1$ the electric field in copper plate 2 yields

$$\mathbf{E}' = \underbrace{\mathbf{E}}_{=0} + \mathbf{v} \times \mathbf{B}_1 \,, \tag{2}$$

where $\mathbf{E}'$ denotes the field in the moving frame of reference [19]. As no external electrical fields are taken into account and the choice of an axial symmetrical problem guarantees that no charge builds up due to the interference of eddy currents with material boundaries, the electrical field in the stationary frame of reference $\mathbf{E}$ can be set to zero. Assuming a linear, isotropic and homogenous conductivity σ in the copper plate the current density becomes $\mathbf{J} = \sigma \mathbf{E}'$. The LORENTZ force acting on the copper volume V_{c_2} due to the magnet field then reads as

$$\mathbf{F}_{c_2} = \int_{V_{c_2}} \mathbf{J} \times \mathbf{B} \, \mathrm{d}V = \sigma \int_{V_{c_2}} (\mathbf{v} \times \mathbf{B}_1) \times \mathbf{B} \, \mathrm{d}V \,, \tag{3}$$

yielding a force in z-direction (compare Fig. 1) of

$$F_{c_2,z} = \underbrace{-\sigma v_z \int_{V_{c_2}} B_{r,1}^2 \mathrm{d}V}_{F_{c_2,m_1}} \; \underbrace{-\sigma v_z \int_{V_{c_2}} B_{r,1} B_{r,2} \mathrm{d}V}_{F_{c_2,m_2}} \,. \tag{4}$$

As both magnets contribute to the field, the force can be split up accordingly. F_{c_2,m_1} is the force acting on copper plate 2 caused by the first magnet's field such that a reaction force on magnet 1 of $F_{m_1,c_2} = -F_{c_2,m_1}$ can be defined. The force F_{c_2,m_2} is caused by the interaction of the eddy currents with magnet 2 and an equivalent reaction force $F_{m_2,c_2} = -F_{c_2,m_2}$ is acting on it. Owing to the symmetry the force acting on the stationary copper plate $F_{c_1,z}$ equals $F_{c_2,z}$ in amplitude but differs in sign and again corresponding reaction forces can be defined

$$F_{c_1,z} = F_{c_1,m_1} + F_{c_1,m_2} = -F_{c_2,z} \,. \tag{5}$$

Summing up all damping forces which act on the moving parts

$$\begin{aligned} F_{2,z} &= F_{c_2,z} + F_{m_2,z} = F_{c_2,m_1} + F_{c_2,m_2} + \underbrace{F_{m_2,c_1}}_{=F_{c_2,m_1}} + \underbrace{F_{m_2,c_2}}_{=-F_{c_2,m_2}} \\ &= 2\,F_{c_2,m_1} = -2\sigma v_z \int_{V_{c_2}} B_{r,1}^2 \mathrm{d}V \,, \end{aligned} \tag{6}$$

all terms of mixed fields ($B_1 \cdot B_2$) cancel out as they only contribute to separating forces between copper plate and magnet assembled in one half of the damping element. Taking the rotational symmetry and the geometric dimensions depicted in Fig. 1 into account, the integral in Eq. 6 can be simplified yielding a damping force

$$F_\mathrm{d} = -4\pi\sigma v_z \int_{L/2+\delta+a}^{L/2+2\delta+a} \int_0^{r_c} B_{r,1}^2 r \, \mathrm{d}r \mathrm{d}z \,. \tag{7}$$

Due to the repellent orientation of the two magnets, conservative forces also have to be taken into account. To obtain the magnetic force between the two magnets, the magnetization of the second magnet can be substituted by an equivalent current density $\mathbf{J}_\mathrm{m}$ which causes the same flux distribution as the primal permanent magnet [19]. By this means, again the magnetic force can be estimated with use of the LORENTZ force (Eq. 3). The distribution of the equivalent current density $\mathbf{J}_\mathrm{m}$ of the second magnet equals its lateral surface and can be expressed utilizing the well-known delta-function δ_di

$$\begin{aligned} \mathbf{J}_\mathrm{m} &= -M_0 \cdot \delta_\mathrm{di}(r - r_\mathrm{mag})\,\mathbf{e}_\varphi\,; \\ &\quad L/2 + 2\delta + a/2 < z < 3L/2 + 2\delta + a\,. \end{aligned} \tag{8}$$

With the sifting property of the dirac distribution the integral simplifies to

$$F_\mathrm{mag} = \int\limits_{V_{\mathrm{m}_2}} \mathbf{J}_\mathrm{m} \times \mathbf{B}\,\mathrm{d}V = -2\pi M_0 r_\mathrm{mag} \int\limits_{L/2+2\delta+a}^{3L/2+2\delta+a} B_{r,1}(r_\mathrm{mag}, z)\mathrm{d}z\,. \tag{9}$$

Thus, the resulting damper force

$$F_\mathrm{res} = F_\mathrm{d} + F_\mathrm{mag}\,, \tag{10}$$

comprises a dissipative part which depends linearly on the velocity and quadratically on the flux density and a conservative part which depends linearly on the flux density.

As the flux density of a cylindrical permanent magnet can be formulated analytically employing Elliptic Integrals (see Eq. 13 in Appendix) but no analytic solutions are known for those integrals, the expressions of F_d and F_mag can only be validated numerically. For the comparison with the finite element based solution, this semi-analytical approach is carried out using an adaptive Lobatto quadrature integration scheme. For this purpose any standard software for numerical calculus is appropriate.

3 FINITE ELEMENT MODELING

To obtain the analytical expressions for the damping element's properties presented in the previous section, some constraining assumptions had to be taken into account. That is, only rotationally symmetrical geometries and motion in axial direction have been regarded. A relative permeability of $\mu_\mathrm{r} = 1$ was assumed in the whole problem region, i.e. no ferritic steel is considered. In the future application those assumptions might not hold as magnets and copper plates have to be integrated into the turbine blades so that they do not interfere with the aerodynamic behavior of the assembly. In structural dynamics any direction of motion has to be considered. Therefore, in the following an electromagnetic finite element analysis of the damping element is carried out. Regarding the above presented academic case of a 2D rotational symmetrical problem the finite element results are compared to the analytical solution and validated experimentally to ensure the computational approach for a future analysis of real geometries.

One key aspect of this finite element based approach is that in a transient electromagnetic computation the whole problem region has to be meshed including surrounding air layers. Nevertheless, motion of electrical conductors or magnetic field sources have to be taken into account such that a mesh adaption has to be fulfilled during time stepping. To the author's knowledge no such analyses have been carried out concerning vibration suppression strategies. But publications covering the connection of electromagnetic forces and motion can be classified into the fields of eddy current braking systems, linear motors, levitation systems and rotational machines. In the following a few of those publications are mentioned with a focus on the applied solution for that issue.

ALBERTZ ET AL. [20] studied an active eddy current braking system of a high velocity train using the FEM. As only transversal motion along an infinitely long rail was assumed, the steady-state results could be obtained using a magnetostatic potential formulation. The velocity effect was thus incorporated by adding $\mathbf{v} \times \mathbf{B}$-terms (see Eq. 2) to the electrical field. The braking force was computed with respect to the velocity of the train for a nonlinear yoke material. The results were validated with measurement data. NIIKURA ET AL. [21] studied a similar setup using the FEM. However, they took the transient effects into account by moving a constant source magnetic field along a finite conductor. The source field was directly impressed so that the actual source, e.g. a permanent magnet did not have to be included in the model and, thus, relative motion between meshed bodies was not addressed in this paper.
ONUKI ET AL. [22] examined a single-sided linear induction motor by means of a 3D transient FEM. They compared the dependency of the thrust force on the position of the moving part for different configurations and discussed various transient phenomena. A 1-DOF mechanical model and an electric circuit model were coupled to the electromagnetic field analysis. WEGENER [23] computed the magnetic field and the forces in a tubular permanent magnet linear motor. His nonlinear 2D axial-symmetric and 3D analyses, however, only considered the quasi-stationary state. The field quantities were, therefore, obtained by a static parametric study of the position instead of a transient analysis including actual motion. VESE ET AL. [24] carried out nonlinear 2D axial-symmetric FE analyses of a linear motor. They considered time-harmonic as well as transient cases and calculated magnetic flux, electromagnetic forces acting on the moving part of the motor and thermal loss. KURZ ET AL. [25], [26] examined the transient behavior of an electromagnetic levitation system, consisting of an aluminum plate above two concentric current-carrying coils. The 3D

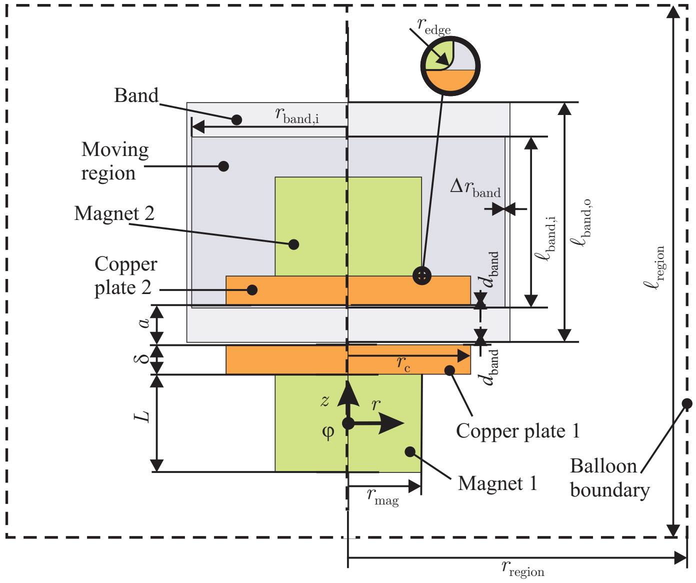

FIGURE 2. 2D AXIALLY SYMMETRIC FINITE ELEMENT MODEL CONSISTING OF MAGNETS, COPPER PLATES, MOVING REGION, BAND AND BALLON BOUNDARY

nonlinear model was analyzed by a hybrid FEM/BEM strategy. While the interior of the conducting and permeable objects were described by finite elements in their respective frames, the surrounding air space was considered by means of boundary elements in the laboratory frame. The FEM/BEM coupling includes the transformation rules between the different frames. Mechanical and electromagnetical models are weakly coupled in order to account for transient dynamic effects. Unfortunately, no experimental validation was provided. LAI ET AL. [27] studied a 3D setup similar to the one presented by KURZ ET AL. [25] using the FEM. General motion is taken into account by a so called 'LAGRANGE sliding interface approach' which couples individually meshed stationary and moving objects. Meshes are specified as either master or slave meshes. The continuity of field components at the interface of both meshes is ensured employing LAGRANGE multipliers. The dynamics of the levitating disc is modeled as a mechanical 1-DOF system. Transient dynamic results are validated by measurements. RACHEK AND FELIACHI [28] also analyzed the transient behavior of a 3D levitation system model by means of the FEM. In contrast to [27], the authors proposed to include the effect of motion by a 'Fast Partial Remeshing Technique'. Only the mesh in the area between the stationary and the rigid moving object is remeshed at each time step.

Finite element model. In the analyses presented in this paper the electromagnetic field calculations were carried out separately from structural mechanics in a transient analysis in the time domain. To account for the change of geometry, a rigid body motion of one half of the damping element was applied. A commercial finite element code was used which allowed for the consideration of motion by applying a remeshing between different time steps [29]. The symmetry of the problem regarding geometry, material and motion was utilized to reduce the general 3D problem to an axially symmetric 2D problem (Fig. 2). Permanent magnets and copper plates were modeled as distinct bodies for which the material properties could be assigned individually. For the outside of the problem region, balloon boundaries were applied. The elements along the balloon boundary are infinity elements that treat the problem region as spreading out towards infinity [29]. To accomplish mechanical excitation, an arbitrary function of time can be specified for rigid body motion in axial direction. Eddy current effects were considered in both the copper plates and the permanent magnets. The software provides a band-type mesh regeneration for the consideration of rigid body motion. The band object separates the moving object from the stationary surrounding area. In each time step of the transient analysis, the band object is remeshed whereas the meshes of moving region and stationary objects are kept fixed. The fixed meshes for stationary and moving objects are linked from a static analysis. In the static analysis, adaptive mesh refinement is applied. The geometric variables and material properties are listed in Tab. 1.

Mesh convergence study. In order to evaluate the accuracy of the finite element model and the program's adaptive mesh refinement capabilities, a mesh convergence study in a static analysis was performed. In general only triangular elements with first order shape functions are used for the calculation of the vector fields. For adaptive mesh refinement, the solver automatically determines the regions with the largest error energies and refines them by splitting up in smaller elements. In Fig. 3 the finite element mesh is depicted after the fourth iteration (not converged yet). The maximum edge length inside the band object is actively controlled so that it never exceeds the average edge length of the interface elements [29]. In particular the area in the vicinity of the edges of the permanent magnets has been intensely refined. Apparently the edges represent so called 'hot-spots' for the FEA. Learning from that, a slightly modified model was considered where all sharp edges which represent a geometrical singularity have been replaced by a small radius of $r_{\mathrm{edge}} = 0.25\,\mathrm{mm}$. To validate the quality of the current mesh the resulting force has been considered instead of the overall energy error. As the force depends on the derivative of the magnetic field it converges more slowly. In addition to that, the forces may

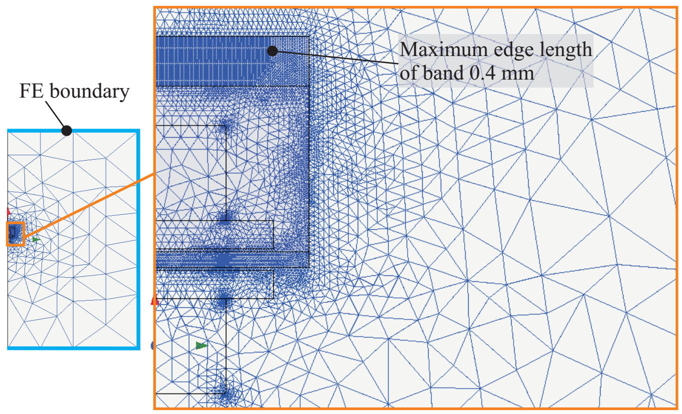

FIGURE 3. FINITE ELEMENT MESH AFTER FOURTH ITERATION (NOT FINAL); LEFT: FULL REGION; RIGHT: DETAIL

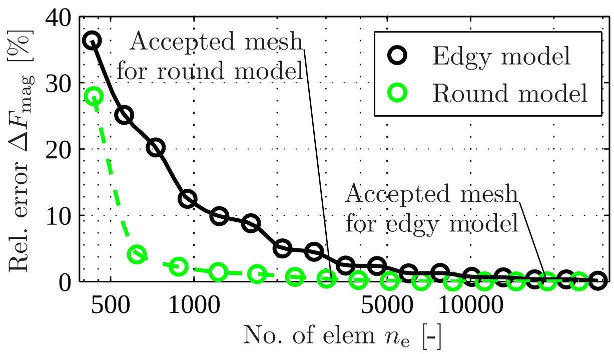

FIGURE 4. FORCE CONVERGENCE

require a higher local accuracy. Comparatively large local errors, however, might not be detected by a global error function. Since the forces are crucial for the mechanical interaction, a tolerance of 1 % was specified for the relative change in the resulting force between two consecutive adaptive refinement iterations. In Fig. 4 the resulting force error for both models is depicted. Apparently the model with additional artificial radii converges much faster such that only 3000 instead of 17000 elements are necessary for the specified accuracy resulting in a speed-up of a factor of 8 with only a difference in the resulting force of 0.03 %.

Transient analysis. In the transient analysis an imposed harmonic velocity with a constant amplitude and frequency was specified for the axial motion of the moving parts of the damper configuration. The program applies homogeneous initial conditions to the motionally induced eddy currents. In order to accomplish fast convergence of the transient hysteresis cycle, it is therefore reasonable to choose the initial conditions accordingly. A velocity of zero for $t = 0$ is chosen so that homogeneous initial

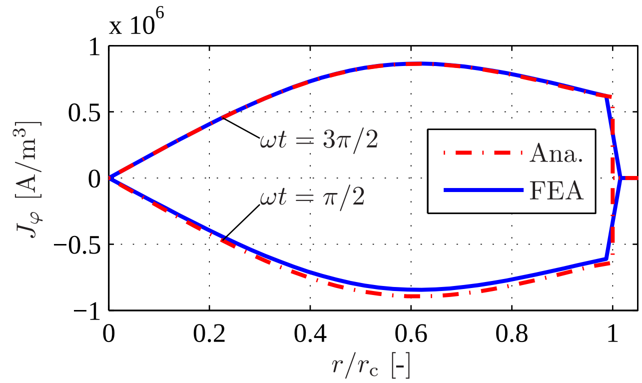

FIGURE 5. EDDY CURRENT DISTRIBUTION J_φ WITH RESPECT TO RADIAL POSITION (MIDPLANE OF THE COPPER PLATE) AT $\Delta z = a$ FOR VELOCITIES $v(\omega t = \pi/2) = v_0$ AND $v(\omega t = 3\pi/2) = -v_0$

conditions are a good approximation, at least for low frequencies. Velocity v and air gap Δz of the moving parts are therefore defined as

$$\begin{aligned} \Delta z(t) &= a\,(1 - \beta \cos \omega t) \\ v(t) &= v_0 \sin \omega t = a\beta\omega \sin \omega t = \Delta \dot{z}(t)\,. \end{aligned} \tag{11}$$

Herein, a denotes the static air gap, β is the amplitude ratio with $0 \leq \beta \leq 1$, and $v_0 = a\beta\omega$ is the magnitude of the velocity. The initial position of the defined motion is thus the lower reversal point which coincides with the position for the linked static analysis. By tracking the force error convergence with respect to the number of time steps per period, it was found that a constant time step using 64 sampling points delivers a good trade off between accuracy and computational efficiency. Due to hysteresis effects in conjunction with homogenous initial conditions for the induced eddy currents, the transient solution will generally not be periodical after computing the first period. Thus, to ensure steady state conditions, a tolerance of 0.5 % was specified for the periodicity criterion ($\Delta F = [F(t) - F(t-T)]/F(t)$). The vibration frequency was found to be the major influence parameter. For frequencies up to $f = 200$ Hz steady state conditions can be ascertained in the third period.

As a first result the current density distribution at the midplane of the copper plate is presented in Fig. 5 for the maximum and minimum velocities when crossing the static air gap. For a radius of $r = 0$, the current density is identical to zero since the radial magnetic flux density is zero on the z-axis. It increases for small radii until it reaches a maximum. For larger radii, the current density is decreasing again until there is a step at the interface between copper and vacuum, i.e. at the outer radius of the copper plate $\frac{r}{r_c} = 1$ due to the conductivity discontinuity. The analytical solution delivers identical results for both extrema of velocity which differ only in their sign. This does not hold totally for the finite element based solution. Apparently the $\mathbf{v} \times \mathbf{B}$-term (Eq.2) is not the only cause for a current flowing in the copper plates. The reason for this are probably inductive effects of the copper plates: The current will cause an electromagnetic field that counteracts the current decay and growth in the copper plate. Although this phenomenon is relatively small for moderate frequencies it is noteworthy as it indicates another constraint of the analytical solution in terms of high frequencies.

In Fig. 6 the forces acting on the moving copper plate, the moving magnet and the resulting force of that assembly are depicted in time and frequency domain. When regarding the copper plate's force (blue curve) it becomes apparent that the dissipative part is not strictly harmonic. Besides the first harmonic which corresponds to the excitation frequency, a moderate second harmonic is present which equals approximately 25 % of the first harmonic. In the time interval in which the copper plate is moving in the stationary magnet's vicinity ($0 \leq \tau \leq \frac{1}{2}\pi$, $\frac{3}{2}\pi \leq \tau \leq 2\pi$), it experiences a higher flux density. Thus, higher eddy currents and forces are induced than in the other half period resulting in a stretched/compressed sine inducing higher harmonics. Also it can be seen that the force does not vanish for a velocity of $v(\tau = \pi) = 0$ resulting in a constant offset. That again indicates inductive effects. The magnet force (red curve) is not only the magnetostatic force between the opposing magnets but also the reaction force associated to the stationary copper plate. Thus, the magnet force is also subject to a phase shift and is not only a function of the displacement anymore. Therefore, it becomes hard to analyze the magnet force due to the interference of these different effects. The resulting force (green curve) is simply the sum of the copper force and the magnet force. Since the copper force and the magnet force apparently have a phase difference in their first harmonic, the first harmonic amplitude of the resulting force is not much larger than the one of the magnet force. Despite the monoharmonic excitation, the resulting force reveals a comparatively high distortion. Hence, the strong nonlinearities of the magnetic field yield a nonlinear behavior of the damper.

Equivalent dynamic parameters. To evaluate the dampers' performance in terms of structural dynamics, despite the nonlinearities presented in the previous section, linear equivalent parameters such as stiffness and damping constant shall be derived in the following.

Based on the first harmonic amplitudes of the resulting force equivalent stiffness and damping coefficients c_{eqv} and d_{eqv} are calculated by applying the harmonic balance method. Regarding the kinematics of Eq. 11 according to [30] the equivalent stiffness and damping coefficients, c_{eqv} and d_{eqv} can be computed

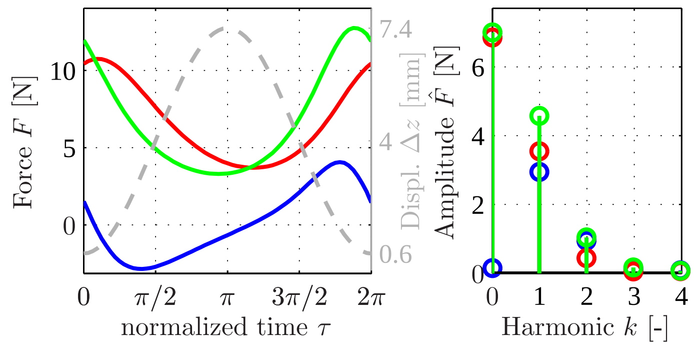

FIGURE 6. TRANSIENT FORCES OF COPPER PLATE (BLUE), MAGNET (GREEN) AND RESULTING FORCE (RED) IN TIME AND FREQUENCY DOMAIN; $a = 4\,\text{mm}$, $\beta = 0.85$, $f = 200\,\text{Hz}$

as follows:

$$c_{\text{eqv}} = -\frac{\hat{F}_{\text{c},1}}{\beta a}; \qquad d_{\text{eqv}} = \frac{\hat{F}_{\text{s},1}}{\beta a \omega}$$

with

$$\hat{F}_{\text{c},1} = \frac{2}{T} \int_{(T)} F_{\text{res}}(t) \cos \omega t \, \mathrm{d}t; \qquad \hat{F}_{\text{s},1} = \frac{2}{T} \int_{(T)} F_{\text{res}}(t) \sin \omega t \, \mathrm{d}t \,. \tag{12}$$

Based on a parametric study, the linearized parameters are depicted with respect to the static air gap and the amplitude ratio for a frequency of $f = 200\,\text{Hz}$ in Fig. 7. Both of them depend strongly on the static air gap a but only slightly on the vibration amplitude ratio β. The radial flux density of a magnet increases progressively for decreasing distances. Hence, the stiffness which depends on the derivative with respect to the air gap also increases monotonically with decreasing air gaps for a given β. For a larger amplitude ratio and a given static air gap, the damper undergoes a stronger force in the vicinity of the lower reversal point, while it undergoes a weaker force in the vicinity of the upper reversal point. Thus, the magnitude of the force and with that the stiffness is increased. As the damping depends quadratically on the radial flux density (see Eq. 7), it even depends stronger on the static air gap whereas a bigger amplitude ratio only leads to a linearly increased velocity and with that the increase of the damping constant is largely compensated by the normalization with respect to velocity. For a frequency that high a difference of 10.8 % for the stiffness and 11.2 % for the damping between analytical and numerical model has to be stated for the smallest air gap and the biggest amplitude ratio. In case of the stiffness all finite element based values are bigger whereas for the damping they are smaller. The inductive effects of the copper plates discussed in the previous section lead to a delay of the eddy currents and with that to a time shift between resulting force and displacement. Hence, the conservative part which is in phase with the displacement increases whereas the dissipative

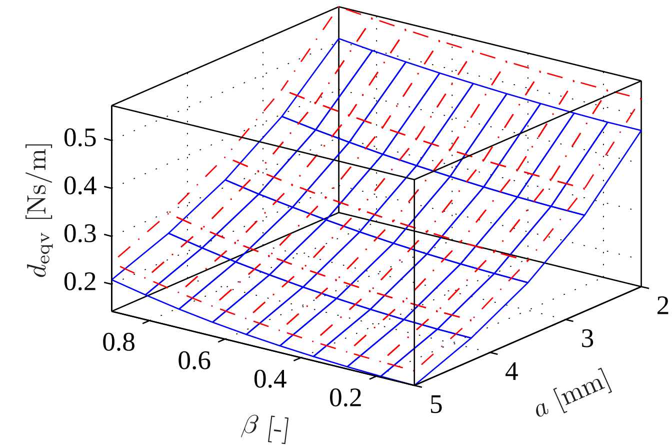

FIGURE 7. FINITE ELEMENT BASED (BLUE) AND ANALYTICAL (RED, DASHED) EQUIVALENT DAMPING CONSTANT d_{eqv} AND STIFFNESS c_{eqv} VS. AIR GAP a AND AMPLITUDE RATIO β; $f = 200\,\text{Hz}$

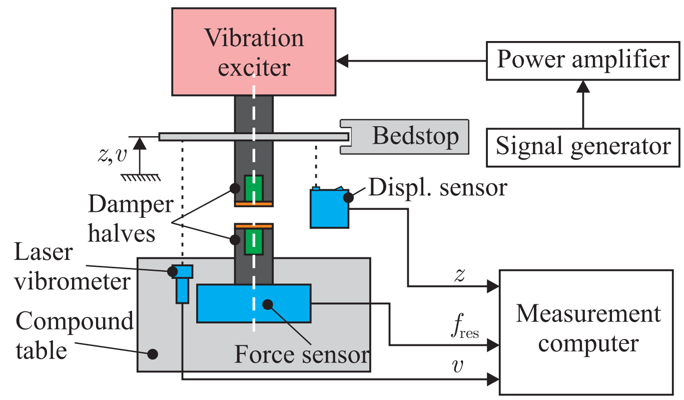

FIGURE 8. TEST RIG FOR THE DIRECT MEASUREMENT OF DAMPING FORCES CONSISTING OF DAMPING ELEMENT VIBRATION EXCITER TO FORCE SINUSOIDAL MOTION AND MEASUREMENT DEVICES

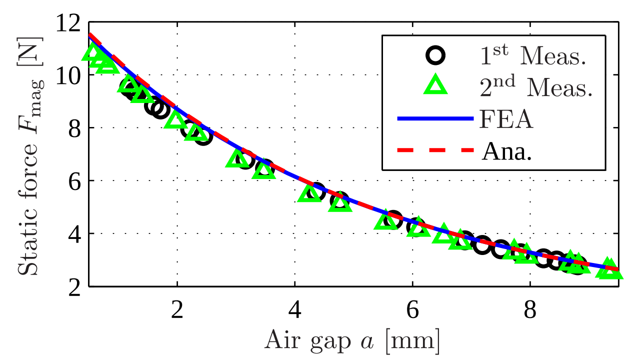

FIGURE 9. STATIC FORCE BETWEEN MAGNETS WITH RESPECT TO AIR GAP

part decreases. This phenomenon was already observed in experiments by BAE ET AL. [31], although they could not predict it with their model.

4 EXPERIMENTAL VALIDATION

The numerical results obtained in the previous sections shall be validated in terms of experiments in the following. Therefore, a first test rig was built to measure the occurring damping forces directly when forcing a sinusoidal motion of one of the two damper halves. Furthermore forced response measurements with a dummy blade pair have been carried out to evaluate the damper's performance.

Measurement of damping forces. The test rig for the direct measurement of the dynamic damper forces is depicted in Fig. 8 schematically. One half of the damping element is mounted on a vibration exciter such that a sinusoidal motion can be impressed. The other assembly of magnet and copper plate is mounted on a stationary force sensor so that the resulting transient forces can be measured. A compound table is used to adjust the air gap a, a displacement sensor and a vibrometer deliver the actual position and speed signal. A sine excitation with variable amplitude, frequency and offset can be specified utilizing a signal generator. The offset is employed for the compensation of a possible static displacement of the exciter's voice coil due to larger static repellent forces. A low pass filter on the force signal is used to suppress noise.

As a first criterion the static magnetic repellent force F_{mag} was measured and compared to the semi-analytical and FE based simulations. Instead of varying the static air gap by manually changing the displacement of the compound table, the measurement data was obtained by a quasistatic analysis. For a

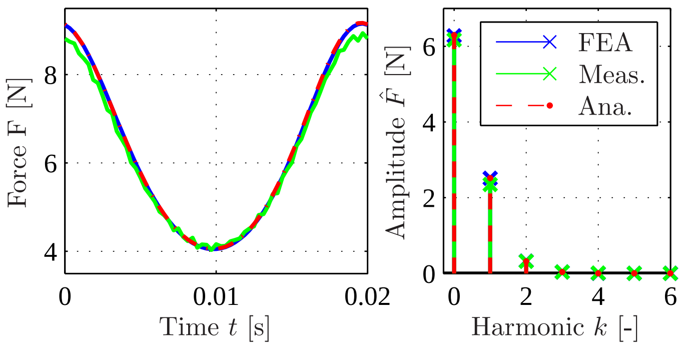

FIGURE 10. ONE PERIOD OF MEASURED AND SIMULATED FORCE IN TIME AND FREQUENCY DOMAIN; $a = 4\,\mathrm{mm}$, $\beta = 0.6$, $f = 50\,\mathrm{Hz}$

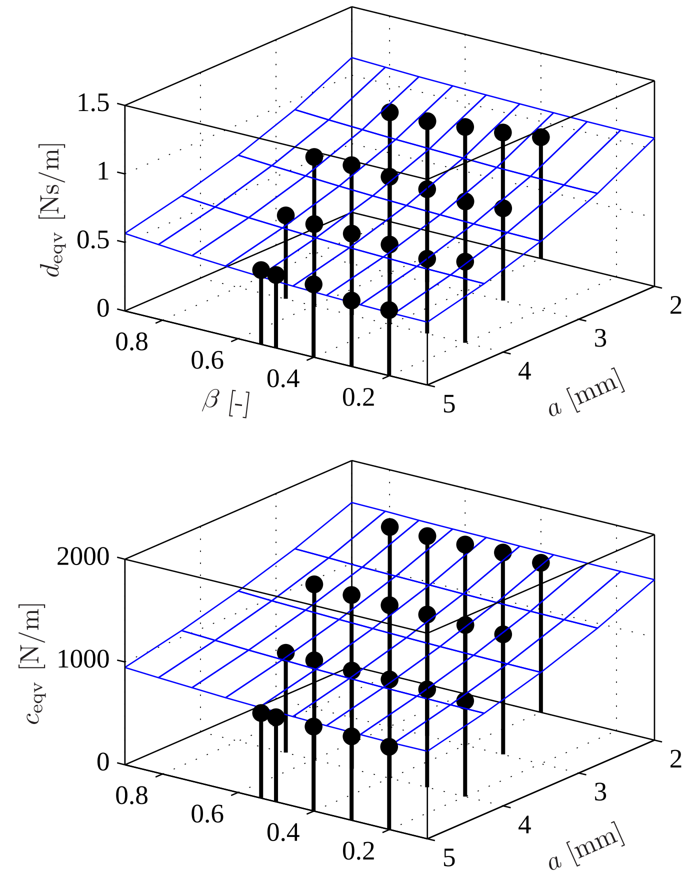

FIGURE 11. COMPARISON OF MEASURED (STEMS) AND SIMULATED (FEA, SURFACE) EQUIVALENT DAMPING CONSTANT AND STIFFNESS; $f = 50\,\mathrm{Hz}$

static air gap of $a = 5\,\mathrm{mm}$ the air gap was thus varied by a sine excitation (amplitude ratio $\beta = 0.9$, frequency $f = 2\,\mathrm{Hz}$) with the shaker resulting in an excellent repeatability. For a frequency that low, transient effects are assumed to be negligible. The static force with respect to the air gap is illustrated in Fig. 9. For this frequency and a moderate relative permeability, the analytical model is a good approximation of the FEA. Measurement and simulation agree well with each other. A maximum relative deviation of 4.7 % between measurement and simulation has been ascertained. An overestimation of the force by the simulation only occurs for small air gaps. One reason for this might be the material nonlinearity which was not considered in the field simulation. Furthermore, geometric imperfections might cause deviations between simulation and experiment. For example, the symmetry axes of both damper parts might deviate, e.g. because of the missing linear slide in conjunction with strong axial forces which would result in stronger deviations for smaller air gaps.

To analyze the dynamic properties of the damping element experimentally, the steady state forces acting on the stationary damper half are measured, when moving its counterpart sinusoidally. Parameter studies have been carried out varying the static air gap a and the amplitude ratio β. To validate the FE model the measured data is compared in time and frequency domain qualitatively which is shown in Fig. 10 for an air gap of $a = 4\,\mathrm{mm}$, an amplitude ratio of $\beta = 0.6$ and a frequency of $f = 50\,\mathrm{Hz}$. Again a good agreement can be observed with slightly smaller peak values in the measured data. It should be noted, however, that the phase is not regarded in the frequency domain which is relevant for the computation of equivalent damping and stiffness properties. For frequencies lower than $100 - 200\,\mathrm{Hz}$, the dissipative part of the damper force is low in comparison to the conservative part. Thus, mainly the conservative part of the force can be compared in Fig. 10.

In particular for the dynamics of the damped structure, the decomposition into the conservative and dissipative parts of the forces or the computation of the equivalent stiffness and damping values is of great importance. The equivalent dynamic properties are compared in Fig. 11 with respect to the static air gap a and the amplitude ratio β. The qualitative behavior of the measured dynamic properties agrees well with the results of the FEA. As predicted they depend strongly on the static air gap a but only slightly on the vibration amplitude ratio β. In accordance with the static results in Fig. 9, the equivalent stiffness is slightly overestimated. The deviation between measurement and simulation increases for smaller static air gaps. In the case of the equivalent damping, larger amplitudes increase this phenomenon. The sign of the deviation is consistent with the ascertained lower radial flux density in the experiment. The damping is quadratically dependent on the magnetic flux density (Eq. 7), whereas the stiffness is only linearly dependent (Eq. 9). Thus, the deviation between measurement and simulation is larger for the damping than for the stiffness due to the error

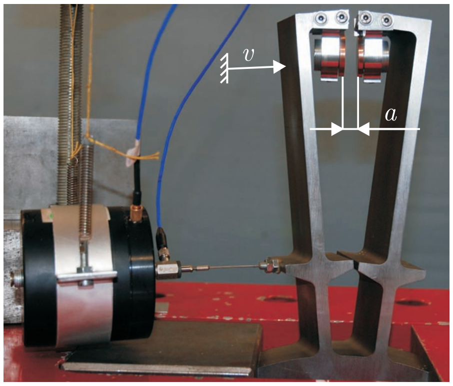

FIGURE 12. TEST RIG FOR FORCED RESPONSE ANALYSES CONSISTING OF DUMMY BLADE PAIR WITH DAMPING ELEMENT VIBRATION EXCITER AND VIBROMETER (NOT SHOWN)

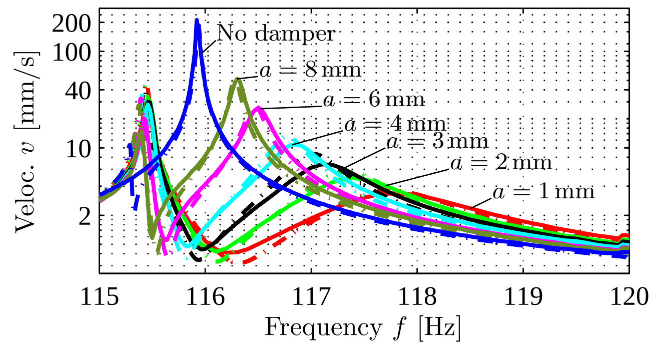

FIGURE 13. FORCED RESPONSE MEASUREMENTS (–) AND SIMULATIONS (–·) FOR DIFFERENT AIR GAPS a

propagation of the magnetic flux density. Also the relatively small dissipative force in comparison to the conservative force for those moderate frequencies increases the uncertainty in the estimation of the damping constants.

Forced response measurements. To evaluate the finite element based equivalent parameters when integrating them in structural dynamics, a recalculation of the forced response measurements presented in [18] based on the newly estimated parameters has been carried out. The test rig is depicted in Fig. 12 and consists of a dummy blade pair, the damping element and an exciter. Measurements have been carried out in the frequency range of the first bending mode of the blades for different air gaps a (Fig. 13). In phase (IP) and out of phase (OOP) mode of the blade pair are that close that only one peak is present when no damper is used. A fraction of critical damping $\xi = 1.41 \cdot 10^{-4}$ has been identified for the system without additional damper. When mounting the damper, the additional stiffness leads to a separation of IP and OOP mode such that two peaks and an antiresonance in between is present. As the stiffness increases with decreasing air gaps, the OOP mode is shifted to higher frequencies slightly. The damper is mounted such that it acts between the blades. Therefore, it does not provide damping with respect to the inertial frame, and only the OOP mode is damped. For the OOP mode an amplitude reduction of 34 dB can be denoted.

To compute the forced response measurements a modal description was applied to a structural finite element model of the dummy blade pair (for details see [18]). To account for the damping element, the equivalent parameters of Sect. 3 have been calculated for a frequency of $f = 115$ Hz and included in a stiffness and viscous damping matrix coupling one DOF of each blade. Good agreement between measurements and simulations can be ascertained. The curves feature the same characteristics and the response levels and frequencies agree quantitatively very well. However small discrepancies in terms of amplitude have to be stated for the intermediate air gaps.

5 SUMMARY AND CONCLUSIONS

In this paper a finite element model of an eddy current based damping device for the reduction of turbine blade vibrations was presented. In transient analyses the occurring forces have been analyzed when taking sinusoidal motion into account. Nonlinearities have been observed yielding a multi harmonic frequency content. Parameter studies have been carried out, and their influence on the most important parameters such as damping constant and stiffness has been analyzed. The finite element model was experimentally evaluated by directly measuring the resulting forces and by means of forced response analyses. Good agreement between measured and simulated vibration amplitude can be ascertained such that despite the observed nonlinearities equivalent linear parameters can be used in the response level prediction.

Comparing the analytical approach with the finite element based equivalent, it can be stated that the analytical approximation delivers comparable results when regarding the restricted case of moderate frequencies, only axial motion and no high permeable objects in the magnet's vicinity.

In future analyses the finite element model will be used to study the observed inductive effects in detail such that also higher frequency modes can be analyzed precisely. Also it will be examined whether an adoption concerning surrounding ferritic steel and arbitrary motion in a 3D analysis is feasible to account for boundary conditions with a practical orientation.

REFERENCES

[1] Swedowicz, J., 2010. "30-Year anniversary of friction damper technology in turbine blades". *Mechanical Eingineering Magazine*, April.

[2] Yang, B.-D., and Menq, C.-H., 1997. "Modeling of friction contact and its application to the design of shroud contact". *Journal of Engineering for Gas Turbines and Power,* **119**(4), pp. 958–963.

[3] Griffin, J. H., 1980. "Friction damping of resonant stresses in gas turbine engine airfoils". *Journal of Engineerig for Power,* **102**, pp. 329–333.

[4] Sanliturk, K., Ewins, D., and Stanbridge, A., 2001. "Underplatform dampers for turbine blades: theoretical modeling, analysis, and comparison with experimental data". *Journal of Engineering for Gas Turbines and Power,* **123**, p. 919.

[5] Panning, L., Popp, K., Sextro, W., Götting, F., Kayser, A., and Wolter, I., 2004. "Asymmetrical underplatform dampers in gas turbine bladings: theory and application". *Transactions of the ASME Turbo Expo 2004*, June.

[6] Laxalde, D., Gibert, C., and Thouverez, F. "Experimental and numerical investigations of friction ring damping of blisks". *Proceedings of the ASME Turbo Expo 2008*.

[7] Chen, J. J., and Meng, C. H., 1999. "Prediction of periodic response of blades having 3d shroud constraints". *Transactions of the ASME Turbo Expo 2009*.

[8] Sextro, W., 2000. "The calculation of forced response of shrouded blades with friction contacts and its experimental verification". *Proceedings of the ASME Turbo Expo 2000*.

[9] Firrone, C., Allara, M., and Gola, M., 2008. "A Contact Model for Nonlinear Forced Response Prediction of Turbine Blades: Calculation Techniques and Experimental Comparison". *Transactions of the ASME Turbo Expo 2008,* **2008**(43154), pp. 573–582.

[10] Filippi, S., Rodrigues, E. B., and Gola, M., 2006. "Experimental characterization of contact hysteresis at high temperatures". *ASME Conference Proceedings Turbo Expo 2006*.

[11] Salles, L., Blanc, L., Thouverez, F., and Gouskov, A., 2008. "Dynamic analysis of fretting-wear in friction contact interfaces". *ASME Conference Proceedings Turbo Expo 2008*.

[12] Duffy, K. P., and Mehmed, O.and Johnson, D., 2001. "Selftuning impact dampers for fan and turbine blades". *6th National Turbine Engine High Cycle Fatigue (HCF) Conference Proceedings*.

[13] Sun, J., and Kari, L., 2010. "Coating methods to increase material damping of compressor blades - measurements and modeling". *Proceedings of the ASME Turbo Expo 2010*.

[14] Filippi, S., and J., T. P., 2010. "A methodology for predicting the response of blades with non-linear coatings". *ASME Conference Proceedings Turbo Expo 2010*.

[15] Yen, H.-Y., and M.-H., H. S., 2001. "Passive vibration suppression of beams and blades using magnetomechanical coating". *Journal of Sound and Vibration,* **245**(4), pp. 701–714.

[16] Duffy, K. P., Provenza, A., Trudell, J., and J., M., 2009. "Passively shunted piezoelectric damping of centrifugally loaded plates". *Proceedings of the 17th AIAA Adaptive Structures Conference*.

[17] Hohl, A., Neubauer, M., Schwarzendahl, S., Panning, L., and Wallaschek, J., 2009. "Active and semiactive vibration damping of turbine blades with piezoceramics". *Proceedings. SPIE Smart Structures*.

[18] Laborenz, J., Siewert, C., Panning, L., Wallaschek, J., Gerber, C., and Masserey, P., 2010. "Eddy current damping: a concept study for steam turbine blading". *Journal of Engineering for Gas Turbines and Power,* **132**(5), pp. 052505–1–052505–7.

[19] Cheng, D., 1989. *Field and wave electromagnetics*. Prentice Hall.

[20] Albertz, D., Dappen, S., and Henneberger, G., 1996. "Calculation of the 3D nonlinear eddy current field in moving conductors and its application to braking systems". *Magnetics, IEEE Transactions on,* **32**(3), pp. 768–771.

[21] Niikura, S., and Kameari, A., 1992. "Analysis of eddy current and force in conductors with motion". *Magnetics, IEEE Transactions on,* **28**(2), pp. 1450–1453.

[22] Onuki, T., Kamiya, Y., Fukaya, K., and Jeon, W., 1999. "Characteristics analysis of linear induction motor with two types of secondary structure based on electromagnetic field and electric circuit analysis". *Magnetics, IEEE Transactions on,* **35**(5), pp. 4022–4024.

[23] Wegener, R., 2008. "Zylindrischer Linearmotor mit konzentrierten Wicklungen für hohe Kräfte". PhD thesis, Technischen Universität Dortmund.

[24] Vese, I.-C., Marignetti, F., and Radulescu, M., 2010. "Multiphysics approach to numerical modeling of a permanentmagnet tubular linear motor". *Industrial Electronics, IEEE Transactions on,* **57**(1), pp. 320–326.

[25] Kurz, S., Fetzer, J., and Lehner, G., 1996. "Threedimensional transient BEM-FEM coupled analysis of electrodynamic levitation problems". *Magnetics, IEEE Transactions on,* **32**(3), pp. 1062–1065.

[26] Kurz, S., Fetzer, J., Lehner, G., and Rucker, W., 1999. "Numerical analysis of three-dimensional eddy current problems with moving bodies by boundary element-finiteelement method coupling". *Surveys on mathematics for industry,* **9**(2), pp. 131–150.

[27] Lai, H., Rodger, D., and Coles, P., 2004. "A 3-D overlapping finite-element scheme for modeling movement". *Magnetics, IEEE Transactions on,* **40**(2), pp. 533–536.

[28] Rachek, M., and Feliachi, M., 2007. "3D transient analysis and movement simulation for the modelling of magnetic levitation". *International Journal of Computer Appli-*

cations in Technology, **30**(4), pp. 229–235.

[29] Ansoft, 2009. ANSOFT MAXWELL 12 TECHNICAL NOTES. Tech. rep.

[30] Magnus, K., and Popp, K., 1986. *Schwingungen*. Teubner Stuttgart.

[31] Bae, J., Hwang, J., Park, J., and Kwag, D., 2009. "Modeling and experiments on eddy current damping caused by a permanent magnet in a conductive tube". *Journal of Mechanical Science and Technology,* **23**(11), pp. 3024–3035.

Appendix

Magnetic flux density of a cylindrical permanent magnet

Magnetic flux density of a cylindrical permanent magnet (length L, radius r_{mag}, magnetization M_0) in cylindrical coordinates, coordinate systems' origin coinciding with the magnets center (see [18] for details)

$$\mathbf{B} = \frac{\mu_0 M_0}{2\pi} \int_{-\frac{L}{2}}^{\frac{L}{2}} \frac{\left[K(k) - \frac{2-k^2}{2\left(1-k^2\right)} E(k)\right]\left(z-z'\right)\mathbf{e}_r}{r\sqrt{\left(r+r_{\mathrm{mag}}\right)^2+(z-z')^2}} + \frac{\left[K(k) - \frac{2-\left(1+\frac{r_{\mathrm{mag}}}{r}\right)k^2}{2\left(1-k^2\right)} E(k)\right] r\mathbf{e}_z}{r\sqrt{\left(r+r_{\mathrm{mag}}\right)^2+(z-z')^2}} \mathrm{d}z', \tag{13}$$

where k denotes the modulus and K and E denote Elliptic integrals of first and second kind,

$$\begin{aligned} k^2 &= \frac{4 r r_{\mathrm{mag}}}{(r+r_{\mathrm{mag}})^2+z^2} \\ \mathrm{K}\left(\tfrac{\pi}{2},k\right) &= \int_0^{\pi/2} \frac{\mathrm{d}\psi}{\sqrt{1-k^2\sin^2\psi}} \\ \mathrm{E}\left(\tfrac{\pi}{2},k\right) &= \int_0^{\pi/2} \sqrt{1-k^2\sin^2\psi}\,\mathrm{d}\psi\,. \end{aligned} \tag{14}$$

TABLE 1. PARAMETERS OF THE REFERENCE CONFIGURATION

L	10 mm
δ	3 mm
r_{mag}	7.5 mm
r_{c}	12.5 mm
$\mu_0 M_0$	1.054 T
σ_{m}	1.11 MS/m
σ_{cu}	58 MS/m
$\mu_{\mathrm{rel,m}}$	1.05
$\mu_{\mathrm{rel,cu}}$	0.999991
ℓ_{band}	$1.3\cdot\delta+2a_1$
$\ell_{\mathrm{band,i}}$	$1.3\cdot(L+\delta)$
$\ell_{\mathrm{band,o}}$	$1.3\cdot(L+\delta)+2a_1$
d_{band}	0.3 mm
Δr_{band}	0.05 mm
ℓ_{region}	500 mm
r_{region}	300 mm
r_{edge}	0.25 mm